

東北医科薬科大学

審査学位論文（博士）

氏名（本籍）	ソン ワンリ 宋 万里（中国）
学位の種類	博士（薬科学）
学位記番号	博薬科第 26 号
学位授与の日付	令和 4 年 3 月 8 日
学位授与の要件	学位規則第 4 条 1 項該当
学位論文題名	OGT Regulates β 1,4-GlcNAc-branched N-glycan Biosynthesis Via the OGT/SLC35A3/GnT-IV Axis
論文審査委員	主査 教授 細野雅祐
	副査 教授 関 政幸
	副査 教授 顧 建国

**OGT Regulates β 1,4-GlcNAc-branched *N*-glycan
Biosynthesis Via the OGT/SLC35A3/GnT-IV Axis**

令和 4 年 3 月

東北医科薬科大学大学院薬学研究科

宋万里

Contents

1. Introduction.....	1
2. Materials and methods	3
3. Results	10
4. Discussion.....	23
5. References.....	28
6. Abbreviations	35
7. Acknowledgments	36

1. Introduction

Amongst multiple post-translational modifications (PTMs), protein glycosylation is a common and important process in cells (1-3), and altered glycosylation is a hallmark of many diseases including cancers (4) and diabetes (5). *N*-Glycans are extremely complex and conserved PTMs are found in the secretory pathways of proteins. Thousands of proteins are known to be *N*-glycosylated, which plays a considerable role in processes such as cell-cell and cell-extracellular matrix recognition, the selective localization of proteins, and immune responses (2, 6, 7). Biosynthesis of *N*-glycans in the endoplasmic reticulum (ER) and the Golgi apparatus involves complex machinery and several steps that include enzymatic reactions and transportation. *N*-Glycosylation often associates with other PTMs such as phosphorylation (7) and ubiquitination (8, 9). For example, increases in *N*-acetylglucosaminyltransferase III (GnT-III) produced by E-cadherin lead to a reduced level of phosphorylation in β -catenin through EGF receptor or Src signaling and contribute to the suppression of cancer metastasis (10, 11). One of unique features of *N*-glycans is the GlcNAc-branched complex structure that is sequentially synthesized first by *N*-acetylglucosaminyltransferase I (GnT-I) and GnT-II, and then by GnT-III, GnT-IV, or GnT-V to produce functionally diverse *N*-glycosylated proteins, as shown in Fig 1. Furthermore, GlcNAc-branched structures are reported to be involved in the pathogenesis of type 2 diabetes (5, 12, 13), and in the growth, invasion and metastasis of cancers (14, 15). The loss of GnT-IV provokes endocytosis, which decreases the cell surface residency of Glut2 and contributes to type 2 diabetes (12). Higher levels of GnT-IV expression have been observed in choriocarcinoma (16), hepatocarcinoma (17), and pancreatic cancer (18), which suggests that production by GnT-IV promotes invasion and metastasis. Another important factor that cannot be ignored in *N*-glycan biosynthesis is UDP-GlcNAc, a donor substrate that is produced by the hexosamine biosynthetic pathway (HBP) as an essential substrate in protein

N-glycosylation pathways. UDP-GlcNAc is considered to be a nutritional sensor and an important regulator of cell signaling that concerns cell function (19, 20).

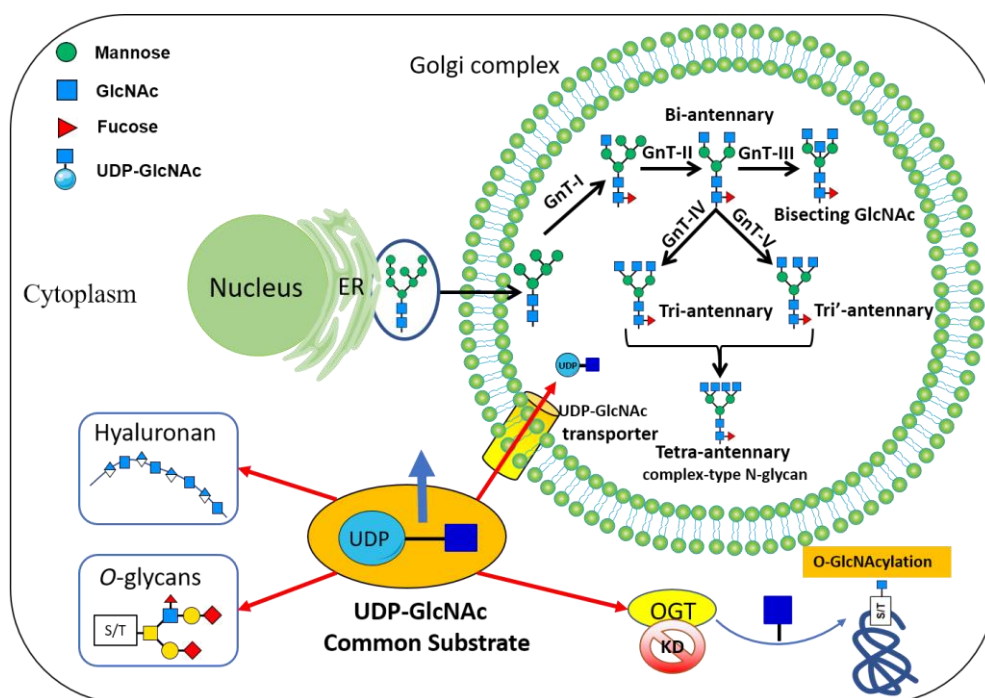


Figure 1. The relationship between *O*-GlcNAcylation and *N*-glycosylation pathway

Unlike the complex *N*-glycans that decorate proteins, *O*-GlcNAcylation is a simple protein PTM, where a single moiety of GlcNAc acts on the serine or threonine residue of target proteins without further elongation or modification into more complex structures (21-23), as shown in Fig 1. *O*-GlcNAcylation is a widespread and dynamic modification that is controlled by only a single pair of enzymes: *O*-GlcNAc transferase (OGT) and *O*-GlcNAcase (OGA). UDP-GlcNAc as a single substrate is used by OGT for *O*-GlcNAcylation. Previous studies have shown that *O*-GlcNAcylation induces a conformational change that initiates protein folding (24), competes with phosphorylation in the same, or proximal, serine or threonine residual (25, 26), disrupts protein-protein interactions (27, 28), serves as a protein recruiting signal (29), and regulates protein stability (30, 31). Furthermore, *O*-GlcNAcylation plays a fundamental role in chronic diseases such as diabetes, Alzheimer's disease, cardiovascular disease, and cancers (25, 32-34). Numerous cancer cells show higher levels of *O*-GlcNAcylation, which makes these cancers more aggressive, and noteworthy examples include prostate cancer (35), leukemia (36), breast

cancer (37), hepatocellular carcinoma (38), and pancreatic cancer (39). The suppression of OGT expression in breast or colon cancer cells decreases cell migration and invasion (40, 41). An increase in the UDP-GlcNAc pool via HBP flux in hyperglycemic cells upregulates *O*-GlcNAcylation (42) and increases the production of GlcNAc-branched *N*-glycans in mammary carcinoma cells (43). Conversely, the loss of OGT in *C.elegans* caused a more than two-fold increase in total UDP-GlcNAc compared with that found in wild type (44). Although amounts of UDP-GlcNAc affect *N*-glycosylation as well as *O*-GlcNAcylation, it is unclear whether there is an interplay between *O*-GlcNAcylation and *N*-glycosylation. It would be reasonable to speculate that suppression of *O*-GlcNAcylation should increase amounts of UDP-GlcNAc for *N*-glycosylation pathways, which would increase the production of GlcNAc-branched *N*-glycans. In the present study, however, we found that OGT knockdown did decrease—rather than increase—the production of β 1,4-GlcNAc-branched tri-*N*-glycans catalyzed by GnT-IV. The main molecular mechanism could be explained by the fact that *O*-GlcNAcylation regulates the stability of SLC35A3, a main UDP-GlcNAc transporter, which specifically interacts with GnT-IV. These findings are the first to describe how *O*-GlcNAcylation specifically governs the biosynthesis of tri-antennary *N*-glycans.

2. Materials and methods

2.1. Antibodies and reagents

The experiments were performed using the following antibodies: biotinylated *Datura stramonium* agglutinin (DSA; B-1185), Concanavalin A (ConA; B-1005), and *Sambucus nigra* agglutinin (SNA; B-1305) ABC kit was acquired from Vector Laboratories; mAb against *O*-GlcNAc (CTD110.6, 9875S) and a peroxidase-conjugated secondary antibody against rabbit (7074S) were from Cell Signaling Technology. Peroxidase-conjugated secondary antibodies against mouse (AP124P) were from Millipore; mAb against α -tubulin (T6199), an antibody against FLAG (F1804), and anti-FLAG conjugated to agarose (Sigma, A2220), VSV (V5507) and anti-VSV-Glycoprotein-Agarose antibody (A1970) were from Sigma; doxycycline hyclate (D9891) was acquired from Sigma-Aldrich; and, cycloheximide (CHX, #037-20991) was purchased from Wako (Tokyo, Japan).

2.2. Cell lines and cell culture

The HeLa and 293T cells were acquired from the RIKEN Bioresource Research Center (Japan). All cells were cultured in DMEM containing 10% fetal bovine serum (FBS, Gibco) under the standard protocol at 37 °C and 5% CO₂.

2.3. Expression plasmids and transfection

We used the Gateway™ cloning system from Invitrogen for all overexpression experiments. The Gateway™ entry vectors were constructed as follows. The cDNA sequences for SLC35A3 were cloned from HeLa cells then inserted into pENTR/D-TOPO vectors with 2 × VSV at the N terminus using the in-fusion method (Takara Bio Inc.). The cDNA sequences of GnT-IVa and GnT-IVb were cloned from HeLa cells and GnT-V was amplified from GnT-V pENTR/D-TOPO vectors in our lab (45) and inserted into pENTR/D-TOPO vectors with 3 × FLAG at the C terminus using the in-fusion method. The resultant cDNAs in entry vectors were confirmed by DNA sequencing. Using LR clonase (Invitrogen), the subcloned cDNAs in entry vectors were transferred into pcDNA3.1-RfA for transient expression. Transfection was performed using PEI MAX (molecular mass, 40 kDa; Polysciences Inc.) following the dictates of the United States patent application (number US20110020927A1) with minor modifications. Briefly, before transfection, 3-5 × 10⁶ cells were seeded on either 10 or 6 cm dishes, and were then incubated for 24 h. Expression vectors with PEI MAX (1 mg/mL in 0.2 M hydrochloric acid) were pre-incubated for 20 min at a 1:3 ratio in 1 mL of a solution that contained 20 mM CH₃COONa buffer and 150 mM NaCl at pH 4.0. After incubation for 6 h, the conditioned medium was replaced with a normal culture medium for further incubation for 48 h.

2.4. Lectin Blot, Immunoprecipitation and Western Blot

The labelled cells were washed with cold PBS and then lysed in the cell lysate buffer (20 mM Tris-HCl, pH 7.4, 150 mM NaCl, 1% Triton X-100) with protease and phosphatase inhibitors (Nacalai Tesque, Kyoto, Japan) for 30 min. Protein concentrations were determined using a BCA protein assay kit (Pierce). An equal amount of protein from each sample was loaded to either 7.5 or 15% SDS-PAGE (sodium dodecyl sulfate-polyacrylamide gel electrophoresis) and transferred to PVDF membranes (Millipore Sigma). The samples were then incubated either

with the indicated primary and secondary antibodies or with biotinylated lectins as indicated. Immunoreactive bands were detected using either an immobilon Western Chemiluminescent HRP Substrate (Millipore) or a Vectastain ABC kit (Vector Laboratories) according to the manufacturer's instructions. For immunoprecipitation, cell lysates (500-1,000 μ g) were immunoprecipitated with anti-VSV-Glycoprotein-Agarose (5 μ L) at 4 $^{\circ}$ C for 2 h with rotation, and then the immunoprecipitates were washed twice with lysis buffer and subjected either to 7.5 or 15% SDS-PAGE, then transferred to PVDF membranes. The membranes were incubated with primary and secondary antibodies as indicated.

2.5. PCR for mRNA expression analysis

Total RNA was extracted from cells using TRIzol Reagent (Invitrogen) according to the manufacturer's instructions. Total RNA (1 μ g) was reverse-transcribed using a PrimeScript RT reagent kit (Takara Bio Inc.). The gene expression levels were detected via RT-PCR, and GAPDH was performed as a control. The PCR primer sequences are listed in supplementary Table 1. PCR amplification was electrophoresed on 1.5% agarose gel in TAE buffer containing 40 mM Tris-acetate and 1 mM EDTA at pH 8.0. Finally, the DNA ladder was visualized with ethidium bromide staining under UV light. The relative expression levels were obtained by quantifying the intensities of the bands from 3 independent experiments and then normalized to GAPDH. And the value of WT cells at 4 h was set as 1.

Table1. Primer sequences for RT-PCR and Real-time PCR

Gene names	Sense primer (5'-3')	Antisense primer (5'-3')
GnT-I	TGACCAGCACCTCAAGTTTATC	CGGAACTGGAAGGTGACAATAC
GnT-II	AGAGTGCCCTGAATGTGATG	CACAGTCTCCAGCATGAAAGA
GnT-III	GCCGCGTCATCAACGCCATCAA	CAGGTAGTCGTCGGCGATCCA
GnT-IVa	GGCTATCACACCGATAGCTGGAG	TCCACCATTCTCTGCAACACC
GnT-IVb	ACAACCCTCAGTCAGACAAGGAGG	GGTACCCTCAGAAGCCCGCAGCTT
GnT-V	GACCTGCAGTTCCTTCTTCG	CCATGGCAGAAGTCCTGTIT
GAPDH	CGGAGTCAACGGATTGGTCGTA	AGCCTTCTCCATGGTGGTGAAGAC
SLC35A2	GTACATATCCCTAGCTGTGCTG	GGTAGGTTAGAGATGGCAACAT
SLC35A3	CAGCTACTTATCAGGTCACGTATC	CTTCAAAGAAACCAAGCTGAAT

2.6. Preparation of *N*-glycans labeled with 2-aminobenzamide (2-AB)

N-Glycan analysis was performed with minor modification, as reported previously (46). The cells ($4\text{--}6 \times 10^7$) were homogenized in 1.5 mL of PBS containing a protease inhibitor mixture (Nacalai Tesque, Kyoto, Japan) using a Potter-Elvehjem homogenizer. The homogenized cell lysates were centrifuged at $1,000 \times g$ for 10 min at 4 °C, and the supernatants were further centrifuged at $100,000 \times g$ for 30 min at 4 °C. Then precipitates were lysed in 100 μ l lysis buffer (20 mM Tris-HCl, pH 7.4, 150 mM NaCl, 50 mM EPPS, 1% Triton X-100) containing protease and phosphatase inhibitors. Protein concentrations were determined using a BCA protein assay kit (Pierce). Same amounts of proteins from each sample (1 mg) were incubated with *N*-Glycosidase F (Takara Bio Inc.) at 37 °C for 72 h according to the manufacturer's instructions and then precipitated with cold ethanol at -20 °C overnight. After centrifugation at $25,000 \times g$ for 20 min, the supernatants containing *N*-glycans were dried via a rotary vacuum evaporator. Those released *N*-glycans were added to Supelclean ENVI-Carb SPE tubes (3.0 mL, 0.25 g; Sigma-Aldrich) and eluted with a mixed solution [50 mM ammonium acetate buffer (pH 7.0)/acetonitrile (40/60)] (47). After drying, *N*-glycans were incubated with 30 μ l of 1 M 2-AB and 0.24 M 2-picoline borane in 10% acetic acid in methanol and purified with HyperSep™ Diol Cartridges (1 mL, 50 mg; Thermo Fisher Scientific).

2.7. Analysis of *N*-glycans by normal and reversed-phase HPLC

To avoid the complexity of the *N*-glycans produced by sialylation and galactosylation, these *N*-glycans were labeled with 2-AB, treated with α 2-3, -6, -8, and -9 neuraminidase A (NEB #P0722, cloned from *Arthrobacter ureafaciens*) and β 1-4 galactosidase (NEB #P0745S, cloned from *Streptococcus pneumoniae*), and then analyzed on a normal-phase HPLC system (JASCO) using an amide-80 HILIC column (250 \times 4.6 mm; Tosoh). Elution was performed at a flow rate of 0.8 mL/min at 45 °C using 0.05% TFA in acetonitrile as solvent A and 0.05% TFA in MilliQ water as solvent B. The column was pre-equilibrated with 30% solvent B, and after injection of a sample for 8 min, the 2-AB-labeled *N*-glycans were separated using a linear gradient of 30–60% solvent B for 120 min. The 2-AB-labeled *N*-glycans were detected using a fluorescence detector (JASCO) at excitation and emission wavelengths of 330 and 420 nm, respectively.

Fractions corresponding to fluorescence peaks were collected and then subjected either to a reversed-phase HPLC or to MS for further analysis. A glucose oligomer ladder (GU) labeled with 2-AB (Agilent) was used as a standard to separate the peaks in the same column under the same conditions, and the GU values are shown at the top of the figure.

ODS-80TM columns (150 × 4.6 mm and 250 × 4.6 mm; Tosoh) were used for reversed-phase HPLC, and elution was performed at a flow rate of 1.0 mL/min at 55 °C using 20 mM of ammonium acetate buffer (pH 4.0) as solvent A and the same buffer containing 1% 1-butanol as solvent B. The column was pre-equilibrated with 4% of solvent B, and after injection of a sample for 10 min, the 2-AB-labeled *N*-glycans were separated employing a linear gradient of 4-100% of solvent B for 60 min. Fractions corresponding to fluorescence peaks were collected and then subjected either to a normal-phase HPLC or to MS for further analysis. The elution patterns of two-dimensional 2-pyridylaminated *N*-glycans on normal and reversed-phase HPLC are very useful for identifying specific *N*-glycan structures (48, 49). For example, when using normal-phase HPLC, the elution time of β 1,4-GlcNAc-branched (tri-antennary) *N*-glycans approximates that of β 1,6-GlcNAc-branched (tri'-antennary) *N*-glycans, while those elution times are quite different in reversed-phase HPLC. The elution time for bi-antennary GlcNAc *N*-glycans was between the times for tri'-antennary and tri-antennary GlcNAc *N*-glycans, as shown in Fig. 4B.

2.8. Analysis of *N*-glycan structures by mass spectrometry (MS)

When the 2-AB-labeled *N*-glycans separated using LC (ODS or Amide column)-FD (fluorescence detection) were dried, each dried residue was dissolved using 20 μ l of a solution of 0.05% trifluoroacetic acid/50% acetonitrile, and a portion of the solution was used for MS and MS/MS analysis as follows. The 2-AB-labeled *N*-glycans were introduced into an ESI source using an Accela HPLC system (Thermo Fisher Scientific) with an injection volume of 5 μ l of a flow solvent solution of 0.05% trifluoroacetic acid/50% acetonitrile with a flow rate of 200 μ l/min without column separation. The *N*-glycan structures were analyzed via LTQ Orbitrap XL (hybrid linear ion trap-orbitrap mass spectrometer; Thermo Fisher Scientific). In the MS setting, the voltage of the capillary source was set at 5.0 kV, and the temperature of the

transfer capillary was maintained at 330 °C. The capillary and tube lens voltages were set at 35 and 130 V, respectively. MS data were obtained in a positive ion mode over a mass that ranged from m/z 350 to m/z 2,500, as measured using orbitrap (resolution, 60,000; mass accuracy, 5ppm). MS/MS data were obtained via an ion trap (data dependent top 3, CID). Xcalibur software ver. 2.2. (Thermo Fisher Scientific) was used to analyze the MS and MS/MS data. Monoisotopic masses were assigned with possible monosaccharide compositions using a GlycoMod software tool (the mass tolerance for precursor ions is ± 0.005 Da, <https://web.expasy.org/glycomod/>), and the proposed glycan structures were further verified via annotation using a fragmentation mass-matching approach based on the MS/MS data, although MS/MS data were not sufficiently obtained due to an insufficient quantity.

2.9. Chemoenzymatic labeling assay

The chemoenzymatic labeling and biotinylation of proteins in cell lysates were carried out using the Click-iT *O*-GlcNAc enzymatic labeling system (Invitrogen). Briefly, the whole cell lysate of 293T cells transfected with an expression plasmid for VSV-SLC35A3 was immunoprecipitated and then labeled with labeling enzymes GalT and UDP-GalNAz according to the Click-iT *O*-GlcNAc enzymatic labeling system protocol (Invitrogen). Labeled proteins were conjugated with an alkyne-biotin compound, once again following the Click-iT protein analysis detection kit protocol (Invitrogen). Control experiments were performed in the absence of GalT and UDP-GalNAz. Biotinylated and control samples were then subjected to 15% SDS-PAGE and transferred to a PVDF membrane for further detection using an ABC kit (Vector Laboratories).

2.10. Assay for protein stability

Analysis of SLC35A3 stability was carried out using a cycloheximide chase assay, as reported previously (50). The inducible OGT-KD-293T cells were transfected with VSV-SLC35A3 for 48 h with or without DOX, and then these cells were cultured with cycloheximide (CHX, #037-20991; Wako, Tokyo, Japan) at a final concentration of 50 $\mu\text{g}/\text{mL}$, and harvested at indicated times. The band densities of VSV-SLC35A3 and α -tubulin on western blots were scanned. Normalization was performed by dividing the VSV signal by the α -tubulin signal at each time

point to determine the percentage of the initial SLC35A3 level (0 h of CHX treatment with the density at 0 h set as 1).

2.11. Establishment of SLC35A3-KO HeLa cells

Lenti-CRISPR v2 was a gift from Feng Zhang (Addgene plasmid #52961) (51). The target site on human SLC35A3 Exon 5 (5'-TCAGCTGGTTCTCAATTTGT-3'), which was chosen from the human GeCKOv2 CRISPR knockout pooled library (52), was cloned into the lentiviral expression vector, and the resultant vectors containing SLC35A3-specific gRNA were confirmed by DNA sequencing. To prepare the viruses, PEI MAX was used to transfect the resultant vector into 293T cells with packaging plasmids. HeLa cells were then infected by the obtained viruses and selected for stable integration with 2 µg/mL puromycin for 72 h. Stable independent clones were isolated using a limiting dilution. The SLC35A3-KO was confirmed by genomic sequences. Genomic DNAs were isolated from several clones of the KO cells, and amplified by PCR using forward primer (5'-AAAGCTCTCCTTTGCAGTCC-3') and reverse primer (5'-GACAAGAGCATTGCCAGATATT-3').

2.12. Enzymatic assays for GnT-IVb and GnT-V

To confirm whether the C-terminally tagged GnT-IVb and GnT-V were still active, enzymatic activities were performed as described previously (53), with minor modification. In brief, 50 µg of enzyme saucers extract from 293T cells transfected with or without (con) expression vector of GnT-IVb or GnT-V, were incubated at 37 °C for indicated times with different buffers as described (53) containing 20 µM pyridylamine-labeled GlcNAc-terminated biantennary glycan (GnGnbi-PA) and 20 mM UDP-GlcNAc in total volume of 10 µL. 30 µL of 10 mM EDTA (pH 7.0) or MilliQ water was added after the incubation, and the enzyme reactions were stopped by boiling for 2 min. Then the reaction mixtures were centrifuged at 20,000 ×g for 15 min at 4 °C. We injected 20 µL of the resulting supernatant into an HPLC system equipped with an ODS-80TM column (250 × 4.6 mm; Tosoh) to separate the products and substrates. The products of GnT-IVb were isocratically eluted at a flow rate of 1.2 mL/min at 50 °C using 50 mM ammonium acetate buffer (pH 4.0) containing 0.12% 1-butanol. The products of GnT-V were isocratically eluted at a flow rate of 1 mL/min at 55 °C using 20 mM ammonium acetate

buffer (pH 4.0) containing 0.1% 1-butanol. Fluorescence was monitored using excitation and emission wavelengths of 320 and 400 nm.

2.13. Wound-healing assay

A wound was scratched into a confluent cell layer on 6 cm dishes using a 200 μ l pipette tip, and after 24 h incubation, the floating cells were gently removed. The cells were further cultured in the medium supplemented with 5% FBS for 24 h. The wound gaps were photographed under a phase-contrast microscope (Olympus, Tokyo, Japan) at 0 and 24 h. The migration distance was evaluated, and then the cell migration rate was quantified relative to the WT (100%).

2.14. Cell proliferation

Cells were cultured at a rate of 2,000 cells per 100 μ L of culture medium per well of 96-well plates and stopped at different times by adding 10 μ L of 5 mg/mL 3-[4,5-dimethylthiazol-2-yl]-2,5-diphenyltetrazolium bromide (MTT; Dojindo, Kumamoto, Japan) with further incubation for 4 h at 37 $^{\circ}$ C. After removal of the medium, 100 μ L of DMSO (Millipore Sigma) was added to dissolve the resultant formazan crystals within the cells. The optical absorbance was assessed at 490 nm using a microplate reader (SpectraMax[®]iD5; Molecular Devices). Cell proliferation rates were determined by relative increases (folds) compared with corresponding cells at the replating time (0 h).

2.15. Statistical analysis

Each experiment included at least three independent procedures. GraphPad Prism[®] 5.0 software (GraphPad Software, Inc., La Jolla, CA) was used for statistical analysis, and $p < 0.05$ was considered statistically significant (*, $p < 0.05$; **, $p < 0.01$; ***, $p < 0.001$; n.s, no significance by two-tail unpaired *t*-test or the analysis of variance (ANOVA) tests).

3. Results

3.1 Changes in the expression levels of GlcNAc-branched *N*-glycans in OGT-KD Cells

First, we used the OGT knockdown (OGT-KD) HeLa cells to investigate *N*-glycan expression via lectin blot. These cells were previously established by the DOX-dependent inducible shRNA KD system in our lab (54). *O*-GlcNAcylation is highly dynamic and often occurs

transiently in response to diverse environmental and physiological cues. Hence, lectin blots were performed at several different time points after cell replating. As shown in Fig. 2A, the *O*-GlcNAcylation levels in the wild type cells (WT) gradually increased at the indicated times, although these levels were persistently suppressed in the OGT-KD cells in the presence of DOX. We believed that a decrease in OGT would increase the production of GlcNAc-branched *N*-glycans in OGT-KD cells. Surprisingly, lectin blot analysis using DSA, which preferentially recognizes β 1,4 linked GlcNAc glycans, showed that the reactive abilities with DSA were decreased in the OGT-KD cells compared with that in WT (Fig. 2B). The underlying molecular mechanism for the increase in *O*-GlcNAc and DSA staining 48-72 h after replating in the WT cells requires further study. On the other hand, the reactive abilities with ConA lectin (Fig. 2C) and SNA lectin (Fig. 2D) did not seem to cause significant changes between OGT-KD and WT cells. These results prompted us to investigate whether OGT-KD alters the expression levels of the glycotransferase genes that are involved in the biosynthetic pathways of GlcNAc-branched *N*-glycans.

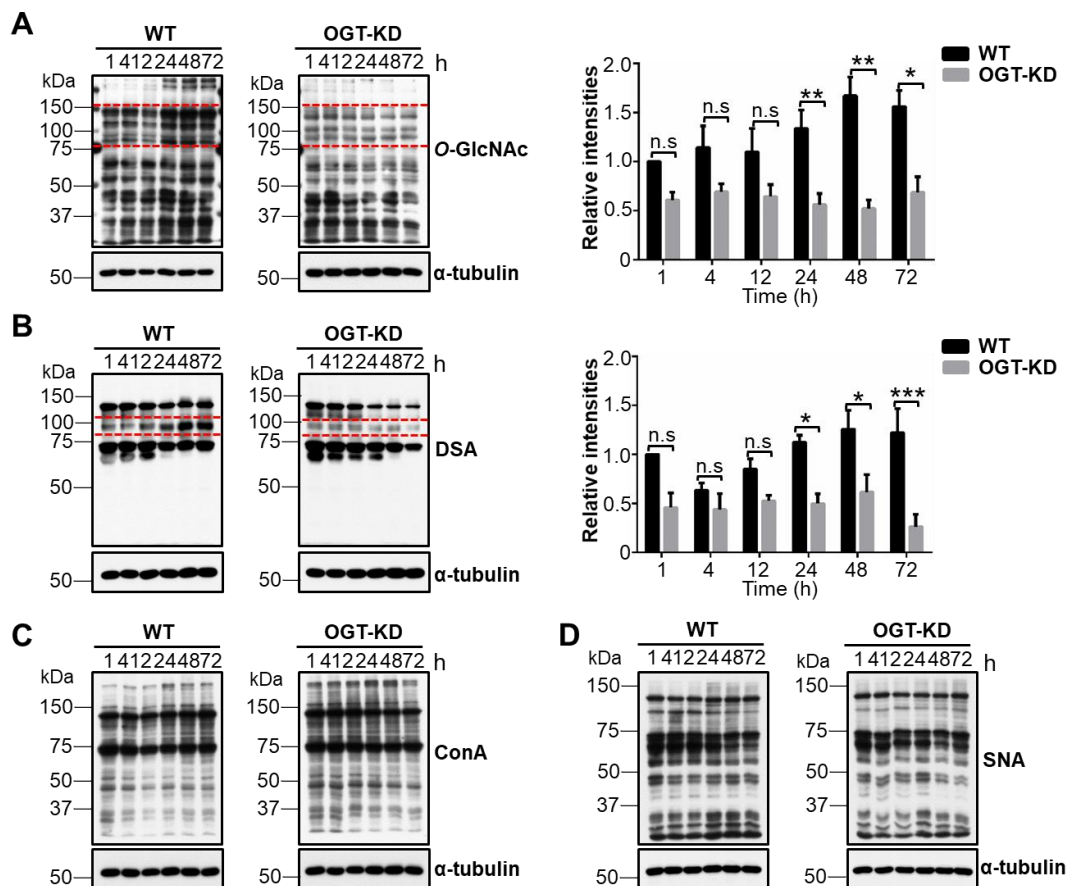


Figure 2. Comparison of glycan changes after cell replating at different times between WT and OGT-KD cells. HeLa cells pretreated with (OGT-KD) or without (WT) DOX at 0.1 $\mu\text{g}/\text{mL}$ for 24 h, were seeded on culture dishes and then harvested at different times as indicated. The same amounts of cell lysates were subjected to 7.5% SDS-PAGE gel and stained either with the indicated antibody or with lectins. A, A representative western blot analyzed by anti-*O*-GlcNAc antibody. The relative intensities were obtained by quantifying the intensities of the bands that fell between 75~150 kDa from 3 independent experiments and then normalized to α -tubulin. And the value of WT cells at 1 h was set as 1. Values represent the mean \pm S.E. *, $p < 0.05$; **, $p < 0.01$; ***, $p < 0.001$; n.s, no significance by two-way analysis of variance (ANOVA). B, Lectin blotting with DSA lectin, which preferentially recognizes β 1-4 GlcNAc-branched glycans. The relative intensities were obtained by quantifying the intensities of the bands that fell between 75~100 kDa from three independent experiments and then normalized to α -tubulin. And the value of WT cells at 1 h was set as 1. Lectin blot analysis with ConA (C) and SNA (D), which preferentially recognizes high mannose types of glycans and α 2,6 sialylated *N*-glycans, respectively.

Results obtained from a semi-quantitative RT-PCR using the primers listed in Table 1, showed no significant differences between the WT and OGT-KD cells after each cell replating at indicated times (Fig. 3).

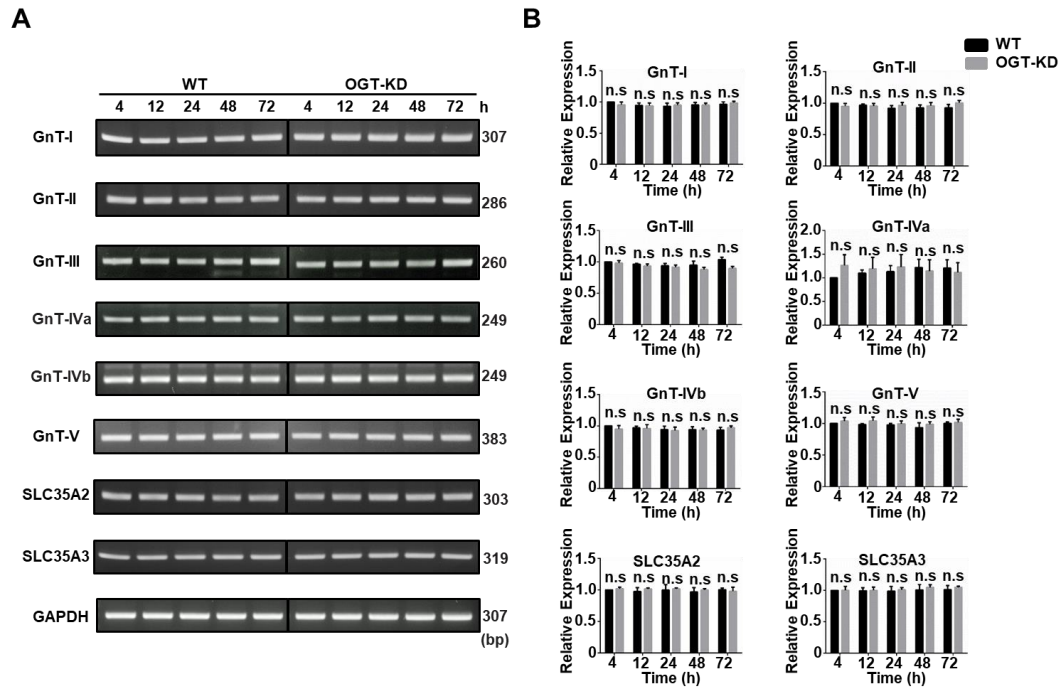


Figure 3. Analysis of mRNA expression levels of GlcNAc-branched *N*-glycan-related *N*-acetylglucosaminyltransferases and UDP-GlcNAc transporters in WT and OGT-KD cells.

Cells were pretreated with (OGT-KD) or without (WT) DOX for 24 h and then seeded on culture dishes which were taken as the 0 h, and then incubated for indicated times. A, the gene expression levels were detected by RT-PCR, and GAPDH was performed as a control. The PCR primer sequences are listed in Table 1. The products of RT-PCR were electrophoresed on 1.5% agarose gel (left panel). The gene expression levels at indicated times were obtained by quantifying the intensities of the bands from 3 independent experiments and then normalized to GAPDH. And the value of WT cells at 4 h was set as 1(right panel). Values represent the mean \pm S.E. n.s, no significance by two-way analysis of variance (ANOVA).

3.2 OGT-KD specifically decreased β 1,4-GlcNAc-branched tri- and tetra-antennary *N*-glycans

To further identify and characterize the GlcNAc-branched *N*-glycan structures, *N*-glycans were released by treatment with PNGase F and labeled with 2-aminobenzamide (2-AB), and further treated with sialidase and galactosidase, as described in the section for “Experimental procedures”. The *N*-glycans then were analyzed via normal-phase HPLC, and each peak was

subjected to mass spectrometry (MS) analysis. The *N*-glycan structures in each peak were verified, as shown in Fig. 4A.

To distinguish the products of GlcNAc- branched *N*-glycans catalyzed by GnT-IV or by GnT-V, each corresponding peak separated in normal-phase HPLC was further subjected to reversed-phase HPLC, and peaks 3, 4, and 5 were further confirmed by MS. Attempts to verify the proposed glycan structures after reversed-phase HPLC were pursued via annotation using a fragmentation mass-matching approach based on the MS/MS data. Although, the tri-antennary glycans were of low abundance precluding acquiring MS/MS spectra of sufficient quality, the elution patterns of two-dimensional 2-pyridylaminated *N*-glycans on normal and reversed-phase HPLC (48, 49), verified that peaks 4, 5 and 6 contained tri-, tri'- and tetra-antennary *N*-glycans, respectively, as shown in Fig. 4B.

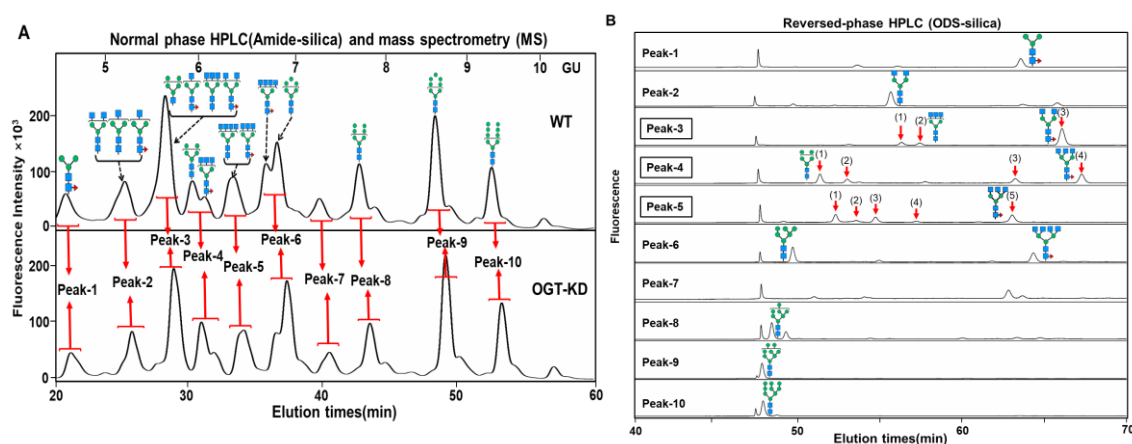


Figure 4. A, The *N*-glycans labeled with 2-AB were prepared as described in the “Experimental procedures” section. After treatment with neuraminidase A and β 1,4 galactosidase, these *N*-glycans were separated by normal-phase HPLC. And then each peak was collected and analyzed by mass spectrometry and verified as *N*-glycan structures based on mass information. The glucose oligomer ladder (GU) labeled with 2-AB was separated in the normal-phase HPLC under the same conditions. B, To determine *N*-glycan structures, each corresponding peak was further subjected to a reversed-phase HPLC, and peak-3, -4, and -5 were again confirmed by mass spectrometry. Based on two-dimensional 2-pyridylaminated *N*-glycans, the elution patterns on normal- and reversed-phase HPLC were determined, as described in the "Experimental procedures" section, as bi-, tri-, tri'-, or tetra-antennary *N*-glycans.

To directly compare these complex types of *N*-glycans, samples were purified by reversed-phase HPLC to remove the high-mannose types and the remaining types of *N*-glycans were then analyzed via normal-phase HPLC. As shown in Fig. 5A, the amounts of β 1,4-GlcNAc-branched (tri-antennary) and tetra-antennary *N*-glycans were lower in OGT-KD cells than in the WT cells. The ratios of tri-antennary or tetra-antennary *N*-glycans versus the sum of the 4 species areas *N*-glycans (bi-, tri-, tri'- and tetra-antennary) consistently showed a significant reduction in OGT-KD cells compared with that in the WT cells (Fig. 5B). By contrast, the ratios of bi-antennary and β 1,6-GlcNAc-branched (tri'-antennary) *N*-glycans in OGT-KD cells showed slightly increase compared with that in WT cells. The data suggest that *O*-GlcNAcylation specifically regulates the biosynthesis of tri-antennary *N*-glycans catalyzed by GnT-IV.

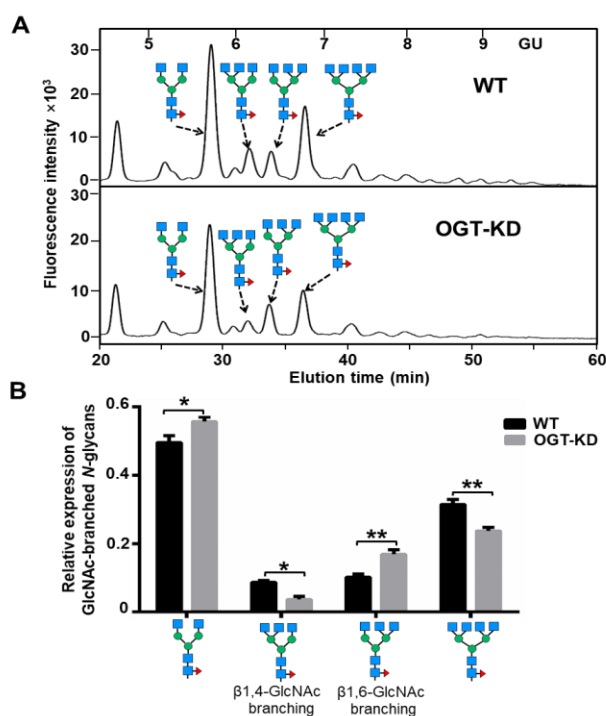


Figure 5. Analysis of GlcNAc-branched *N*-glycans isolated from WT and OGT-KD cells

The *N*-glycans labeled with 2-AB were prepared as described in the "Experimental procedures" section. To avoid complexity from sialylation and galactosylation, these *N*-glycans were treated with neuraminidase A and β 1-4 galactosidase and were further purified by reversed-phase HPLC to remove the high mannose types of *N*-glycans. A, A representative elution pattern for the complex types of major *N*-glycans on a normal-phase HPLC in WT and OGT-KD cells.

Based on analysis using mass spectrometry combined with the two-dimensional elution patterns of *N*-glycans on normal and reversed-phase HPLC as described in the “Experimental procedures” section, the major peaks could be assigned as putative *N*-glycan structures. B, Relative expression of GlcNAc-branched *N*-glycans. The ratio represents each peak area against the sum of the 4 peaks areas (bi-, tri-, tri'- and tetra-antennary *N*-glycans), which was set as 1. The data were obtained from three independent experiments. Values represent the mean \pm S.E. *, $p < 0.05$; **, $p < 0.01$ by two-way analysis of variance (ANOVA).

3.3 SLC35A3, a UDP-GlcNAc transporter, was modified by *O*-GlcNAc

To explore the underlying molecular mechanisms responsible for the effect of *O*-GlcNAcylation on the expression of tri- and tetra-antennary *N*-glycans, we focused on the UDP-GlcNAc transporter. Previous studies had revealed that UDP-GlcNAc transporter KD caused a decrease in the production of tri- or tri'- and tetra-antennary GlcNAc-branched *N*-glycans (55). In addition, SLC35A3 has been considered one of the main UDP-GlcNAc transporters that play important roles in the biosynthesis of complex *N*-glycans (56-58).

Based on the results of those studies, we speculated that the UDP-GlcNAc transporter might be modified by OGT, thereby affecting the biosynthesis of branched *N*-glycans. To test this hypothesis, we constructed an expression vector containing human SLC35A3 tagged with VSV (vesicular stomatitis virus glycoprotein) and overexpressed them in the 293T or DOX-induced OGT-KD 293T cells (54). As expected, western blot analysis showed that SLC35A3 containing either a VSV tag (Fig. 6), was detected by anti-*O*-GlcNAc antibody. *O*-GlcNAcylation levels for SLC35A3 were significantly decreased in OGT-KD cells, compared with those in WT cells (Fig. 6). To further confirm the existence of *O*-GlcNAcylation in SLC35A3, we conducted a chemoenzymatic-labeling assay using an azido-GalNAc sugar, as described in the “Experimental procedures” section, and SLC35A3 was clearly labeled (Fig. 6B). These data proved that SLC35A3 is an *O*-GlcNAcylated protein (Fig. 6).

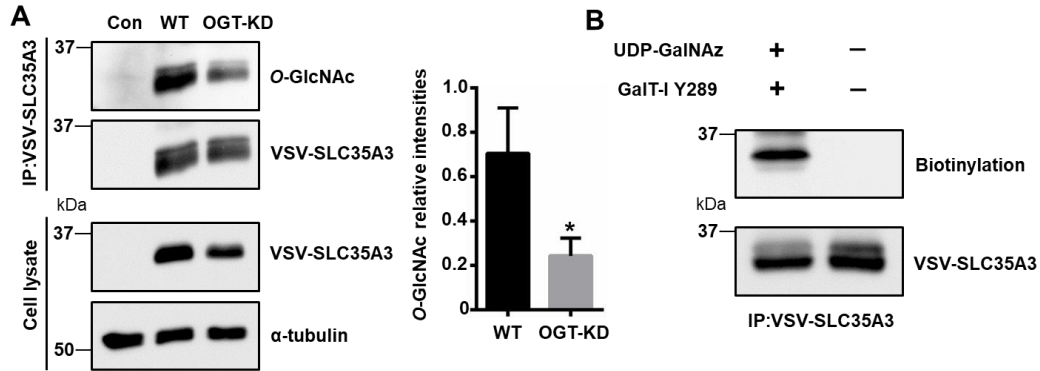


Figure 6. Determination of *O*-GlcNAcylation on SLC35A3. A, 293T cells transfected without (Con) or with VSV-SLC35A3, were incubated without (WT) or with DOX (OGT-KD). The cell lysates and immunoprecipitates (IP) with anti-VSV antibodies were subjected to 15% SDS-PAGE gel and western blotting either with anti-*O*-GlcNAc or the indicated antibodies, respectively. The experiments were independently repeated at least three times. The relative intensity refers to *O*-GlcNAcylated SLC35A3 against total SLC35A3. Values represent the mean \pm S.E. *, $p < 0.05$ (two-tail unpaired t-test). B, Confirmation of *O*-GlcNAcylation on SLC35A3. Cell lysates of 293T cells transfected with SLC35A3 were immunoprecipitated (IP) with anti-VSV antibodies, followed by click chemistry labeling of *O*-GlcNAc residues with (+) or without (-) GalT and UDP-GalNAz, and were detected using an ABC kit as described in the "Experimental procedures" section. The experiments were independently repeated at least three times.

3.4 Suppression of *O*-GlcNAcylation in SLC35A3 reduced its stability

Moreover, we found that the *O*-GlcNAcylation of SLC35A3 contributed to its stability. When cells were treated with cycloheximide, a protein synthesis inhibitor, the decay of SLC35A3 in the OGT-KD cells was significantly faster than that in WT cells (Fig. 7) which suggests that *O*-GlcNAcylation regulates the synthesis of branched *N*-glycans most likely via the modulation of SLC35A3 stability.

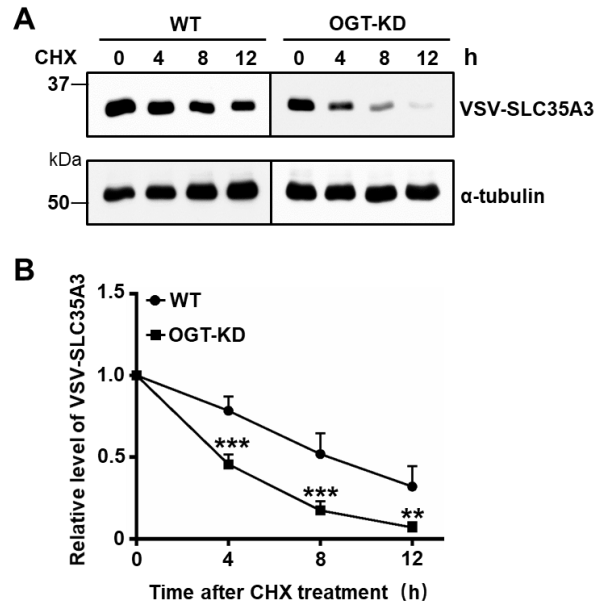


Figure 7. Effect of *O*-GlcNAcylation on SLC35A3 stability. A, 293T cells were transfected with SLC35A3 and were treated without (WT) or with DOX (OGT-KD). After transfection for 48 h, these cells were treated with cycloheximide (CHX), a protein synthesis inhibitor, for indicated times. Total cell lysates were used for western blotting with an anti-VSV antibody. α -tubulin was used as load control. B, Quantitative analysis of the turn-over for SLC35A3. The percentage of SLC35A3 at each indicated time point was normalized by comparing the density with that at time 0, and the density at 0 h was set as 1. The data were obtained from three independent experiments. Values represent the mean \pm S.E. **, $p < 0.01$; ***, $p < 0.001$ by two-way analysis of variance (ANOVA).

3.5. Decrease in the expression levels of tri- and tetra-antennary *N*-glycans in SLC35A3 knockout (SLC35A3-KO) cells

To confirm whether regulation of SLC35A3 is a key factor for the decreased expression of tri- and tetra-antennary *N*-glycans in the OGT-KD cells as described above, we established SLC35A3-KO HeLa cells, which were confirmed by DNA sequencing. Interestingly, decreases in the expression levels of tri- and tetra-antennary *N*-glycans while bi-antennary *N*-glycans increased were also observed in the SLC35A3-KO cells, which is a phenomenon that is similar to that in OGT-KD cells, though tri'-antennary *N*-glycans showed no significant change in the

SLC35A3-KO and WT cells, as shown in Fig. 8. These data further suggest that *O*-GlcNAcylation affects the synthesis of tri- and tetra-antennary *N*-glycans via SLC35A3.

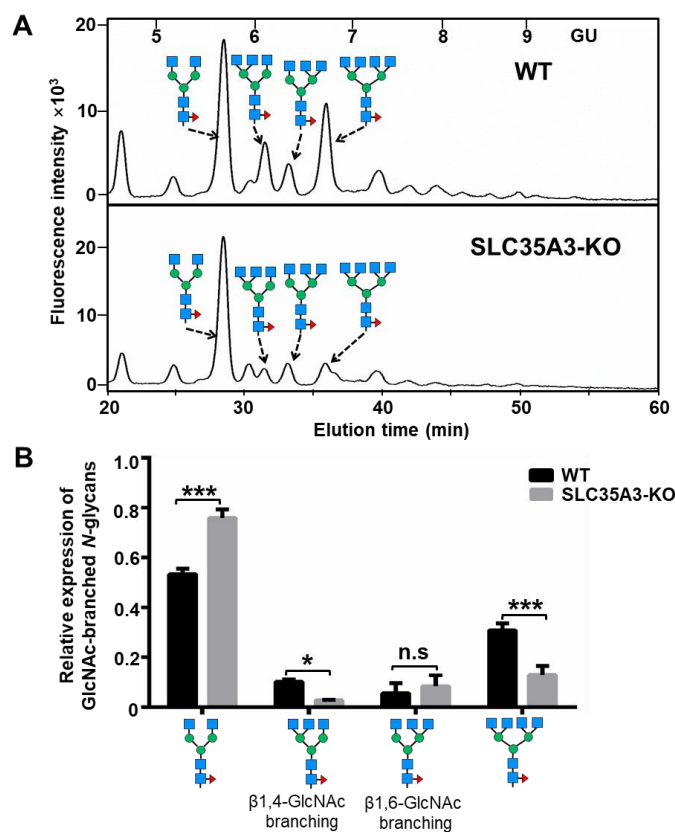


Figure 8. Analysis of GlcNAc-branched *N*-glycans isolated from WT and SLC35A3-KO cells. The methods for the analysis of GlcNAc-branched *N*-glycans are described in Fig.5. A, A representative elution pattern for the complex types of major *N*-glycans on a normal-phase HPLC in WT and SLC35A3-KO cells. B, Relative expression of GlcNAc-branched *N*-glycans. Values represent the mean \pm S.E. *, $p < 0.05$; ***, $p < 0.001$; n.s, no significance by two-way analysis of variance (ANOVA).

3.6 SLC35A3 is specifically associated with GnT-IV

To further understand why SLC35A3-KO resulted in a specific decrease in tri-antennary *N*-glycans, but not in tri'-antennary *N*-glycans, we speculated that there could be an interaction between SLC35A3 and GnT-IV. For this purpose, 293T were transiently transfected with plasmids enabling the expressions of SLC35A3 tagged with VSV and GnT-IVa, GnT-IVb or GnT-V tagged with FLAG. Intriguingly, the immunoprecipitates with anti-VSV antibody

contained FLAG-GnT-IVb (Fig. 9A) or FLAG-GnT-IVa (Fig. 9B), but not FLAG-GnT-V. Since GnT-IVa expression is known to be tissue-specific, whereas GnT-IVb is more ubiquitously expressed (59, 60), so we selected GnT-IVb for further study. Furthermore, we found that OGT-KD decreased the complex formation between SLC35A3 and GnT-IVb (Fig. 9C).

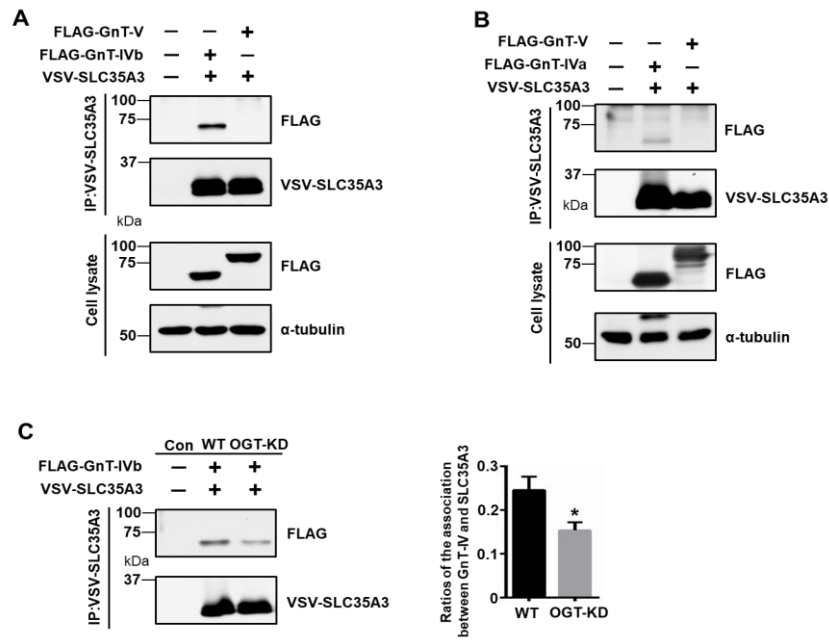


Figure 9. Complex formation between SLC35A3 and GnT-IV.

A, 293T cells co-transfected without (-) or with (+) expression vectors containing SLC35A3 and either GnT-IVb or GnT-V, were immunoprecipitated (IP) by the indicated antibodies. The cell lysates and immunoprecipitates were subjected to 7.5% SDS-PAGE gel and blotted with the indicated antibodies, respectively. B, 293T cells co-transfected with (+) or without (-) expression vectors containing SLC35A3 and either GnT-IVa or GnT-V, were immunoprecipitated (IP) by the indicated antibodies. The cell lysates and immunoprecipitates were subjected to 7.5% SDS-PAGE gel and blotted with the indicated antibodies, respectively. C, Effects of OGT-KD on the interaction between SLC35A3 and GnT-IVb. Cell lysates obtained from the WT and OGT-KD 293T cells that were transfected without (Con) or with expression plasmids of SLC35A3 and GnT-IVb were immunoprecipitated (IP) with an anti-FLAG antibody. The immunoprecipitates were blotted with the indicated antibodies. Ratios of

SLC35A3 in those immunoprecipitates were quantitatively calculated from three independent experiments. Values represent the mean \pm S.E. *, $p < 0.05$ (two-tail unpaired t -test).

The C-terminally tagged GnT-IVb and GnT-V displayed the expected enzymatic activities using pyridylamine-labeled GlcNAc-terminated bi-antennary glycan (GnGnbi-PA) as a substrate (Fig. 10).

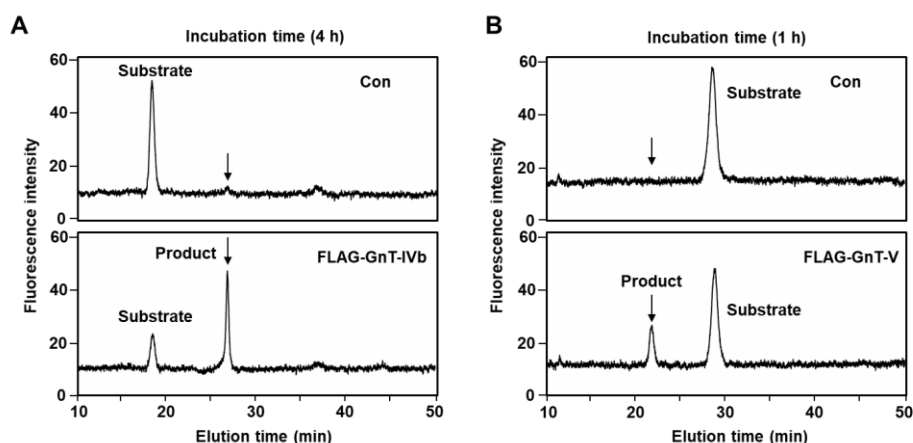


Figure 10. Examination of enzymatic activities for GnT-IVb and GnT-V tagged with FLAG. 293T cells transfected without (con) or with expression vectors FLAG-GnT-IVb (A) or FLAG-GnT-V (B). The same amounts of cell lysates were incubated with acceptor substrate GnGnbi-PA and donor substrate UDP-GlcNAc for indicated times, and the reaction mixtures were analyzed by a reversed-phase HPLC as described in Experimental procedures. Arrows show product positions. A, The products of GnT-IVb were isocratically eluted at a flow rate of 1.2 mL/min at 50 °C using 50 mM ammonium acetate buffer (pH 4.0) containing 0.12% 1-butanol. B, The products of GnT-V were isocratically eluted at a flow rate of 1 mL/min at 55 °C using 20 mM ammonium acetate buffer (pH 4.0) containing 0.1% 1-butanol. Fluorescence was monitored using excitation and emission wavelengths of 320 and 400 nm.

Thus, we concluded that OGT regulates SLC35A3 stability and SLC35A3-GnT-IVb complex formation, which plays a crucial role in the biosynthesis of tri-antennary *N*-glycans.

3.7 OGT-KD and SLC35A3-KO alters cell morphology and inhibits cell migration and proliferation

To gain insight into the roles of OGT in SLC35A3-mediated functions, we further compared the cellular biologic functions between OGT-KD and SLC35A3-KO cells. Our previous study demonstrated that OGT-KD led to an increase in cell spreading and an alteration in the cell shape from elongated spindle shapes to a more rounded morphology (54). A similar phenomenon was also observed in the SLC35A3-KO cells (Fig. 11A). We further used a wound-healing assay to compare the cell migration and found that the wound closure capabilities of both OGT-KD and SLC35A3-KO cells were significantly suppressed, compared with those in the WT cells (Fig. 11B). Moreover, cell proliferation was also significantly decreased in both OGT-KD and SLC35A3-KO cells compared with that in the WT cells (Fig. 11C).

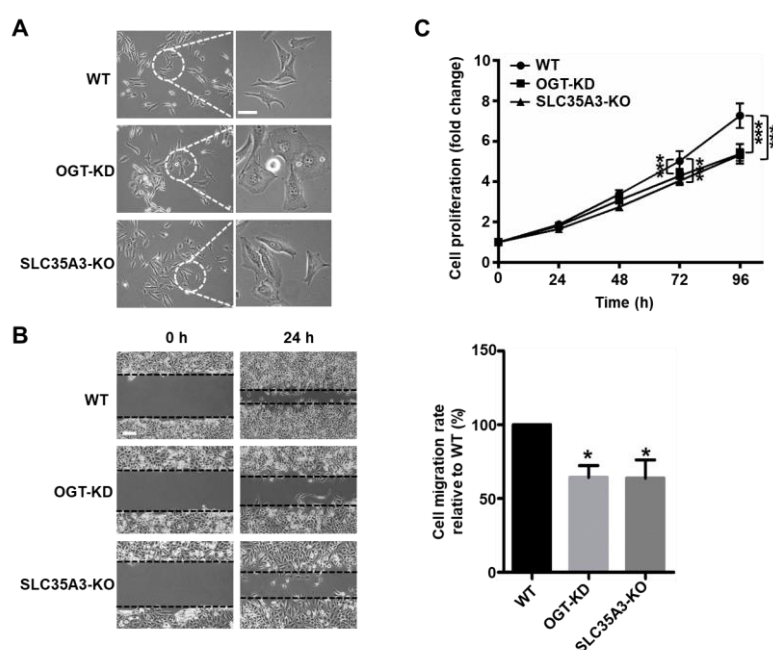


Figure 11. Comparison of effects of either OGT-KD or SLC35A3-KO on cell morphologies, cell migration and proliferation. A, HeLa cells treated with (OGT-KD) or without (WT) DOX, or SLC35A3-KO HeLa cells were pre-incubated for 24 h and then replated on culture dishes. After incubation for 48 h, cells were photographed under a phase-contrast microscope. An enlarged view is shown in the right panel. Scale bars, 15 μ m. B, Cells as indicated were grown to more than 90% confluence, and the monolayers were incised with a

pipette in each well. Photographs were taken by phase-contrast microscopy at 0 and 24 h. The migration distance was evaluated and then the cell migration rate was quantified (right panel). The migration rate for the WT cells was set as 100%. Experiments were independently repeated three times. Values represent the mean \pm S.E. *, $p < 0.05$ by one-way analysis of variance (ANOVA). Scale bars, 50 μ m. C, The WT, OGT-KD, and SLC35A3-KO cells were supplied with DMEM containing 5% FBS seeded on 96-well dishes. The value after incubation for 6 h was set as 0 points (0 h), cells were further incubated, and cell numbers were measured at the indicated times (24, 48, 72, or 96 h) using MTT assay. The relative rate of cell proliferation was shown as increased folds at indicated times compared with that at 0 h, which was set as 1. Experiments were independently repeated three times. Values represent the mean \pm S.E. ***, $p < 0.001$ by two-way analysis of variance (ANOVA).

Taken together, these data functionally support the existence of a novel regulatory mechanism of *O*-GlcNAcylation that impacts the biosynthesis of tri-antennary *N*-glycans via the OGT-SLC35A3-GnT-IV axis.

4. Discussion

In the present study, we clearly showed that *O*-GlcNAcylation interacts with *N*-glycosylation. OGT-KD specifically decreased the biosynthesis of β 1,4-GlcNAc-branched tri- and tetra-antennary *N*-glycans via SLC35A3, a UDP-GlcNAc transporter, and served as a central hub that specifically interacted with GnT-IV. Moreover, suppression of *O*-GlcNAcylation on SLC35A3 affects its stability and the specific complex formation with GnT-IV, which specifically decreases the biosynthesis of β 1,4-GlcNAc-branched *N*-glycans (Fig. 12). However, the specific *O*-GlcNAcylation sites on SLC35A3 requires further study.

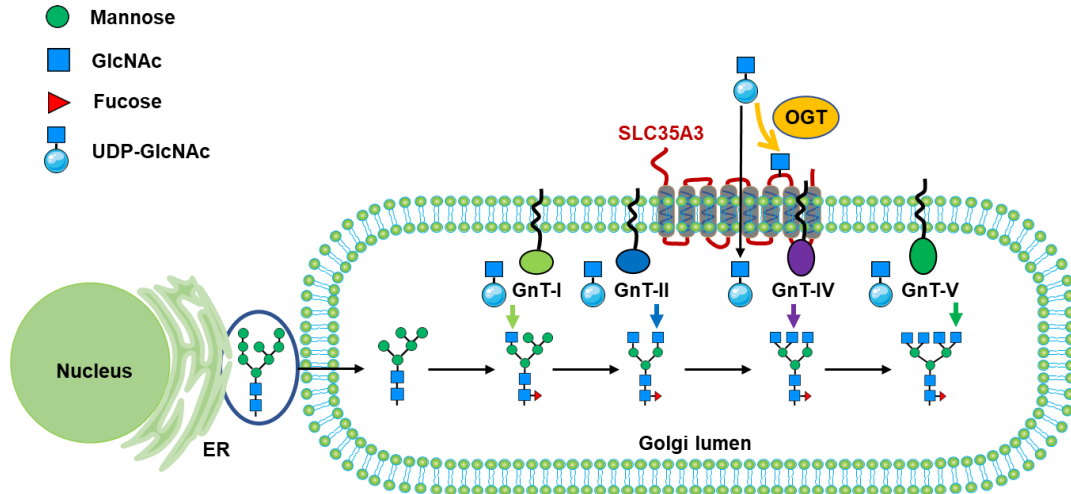


Figure 12. Schematic diagram of the proposed molecular mechanism for regulation of

the biosynthesis of β 1,4-GlcNAc-branched *N*-glycans by *O*-GlcNAcylation. The

specificity for the biosynthesis of these *N*-glycans in OGT-KD cells could also be confirmed using SLC35A3-KO. Furthermore, the effect of SLC35A3-KO on cell adhesion, migration and proliferation was similar to that observed in the OGT-KD cells. Collectively, these results clearly show a novel cross-talk pathway between *O*-GlcNAcylation and *N*-glycosylation via the axis of OGT/SLC35A3/GnT-IV, which may help us to further understand the functions of *O*-GlcNAcylation and the regulation of *N*-glycan biosynthesis.

Generally, different PTMs often coordinate with each other, and *O*-GlcNAcylation is no exception. Given the importance of *O*-GlcNAcylation in multiple fundamental cellular processes, it is reasonable to assume that *O*-GlcNAcylation is involved in the pathological conditions of many diseases such as diabetes, neurological disorders, cardiovascular disease and tumor progression (25, 32, 33). UDP-GlcNAc is an essential common donor substrate for *O*-GlcNAcylation as well as GlcNAc-branched *N*-glycosylation. Complex types of *N*-glycans cannot be fully synthesized without an efficient delivery of UDP-GlcNAc from the cytosol to the Golgi lumen. For example, SLC35A3-KD resulted in a decrease in the amount of UDP-GlcNAc in the Golgi lumen, which reduced the production of tri- and tetra-antennary *N*-glycans (55). The loss of OGT in *C.elegans* caused a more than two-fold increase in total UDP-GlcNAc (44). Thus, *O*-GlcNAcylation may reciprocally interact with *N*-glycosylation through a shared

pool of UDP-GlcNAc. We assumed that the production of GlcNAc-branched *N*-glycans would increase in OGT-KD HeLa cells. However, the results in the present study clearly contradicted our speculation.

Why OGT-KD specifically decreased the tri- and tetra-antennary *N*-glycans is intriguing. Dorota Maszczak-Seneczko et al. previously showed that the silencing of SLC35A3 reduces the GlcNAc-branched *N*-glycans, and then speculated that SLC35A3 might supply UDP-GlcNAc as a substrate mainly for GnT-IV and GnT-V (55). Their assumptions provided a hint that SLC35A3 could be modified by OGT at the cytoplasmic domains since SLC35A3 is a type III multi-transmembrane protein. As expected, OGT did modify SLC35A3 with O-GlcNAc. The O-GlcNAcylation contributed to its stability at the protein level (Fig. 7). Furthermore, SLC35A3-KO specifically decreased the production of tri- and tetra-antennary *N*-glycans, which was partially supported by the results of the previous study of SLC35A3-KD CHO and HeLa cells (55). Although we observed those changes in GlcNAc-branched *N*-glycans in the current study, we believe that O-GlcNAcylation may also modify other transporters besides SLC35A3, resulting in changes in other kinds of *N*-glycans or other glycosylation pathways rather than just the *N*-glycosylation pathway.

However, our observation could not be simply explained by a decrease in UDP-GlcNAc concentrations in the Golgi lumen for GnT-IV and GnT-V in either SLC35A3-KO or OGT-KD cells, because GnT-IV has lower K_m values than those of GnT-V with UDP-GlcNAc as a donor substrate (61). Thus, a decrease in UDP-GlcNAc should have a greater impact on the production of GnT-V compared with that of GnT-IV. Apparently, this was not the case for the present study, as described above. Interestingly, co-immunoprecipitation analysis revealed that SLC35A3 specifically interacts with GnT-IV rather than with GnT-V, which strongly suggests the specificity of SLC35A3 for tri-antennary *N*-glycan biosynthesis and further supports our observations. The FRET approach in A375 and 293 cells, however, showed that SLC35A3 and GnT-V seemed to be close in the Golgi membrane, although the association could not be detected by co-immunoprecipitation (55, 62). Whether the difference is due to cell lines, to association strength between molecules, or to other mechanisms involved will require further

study. In addition, we also noticed that the increase in O-GlcNAc and DSA staining 48-72 h after replating, but the mRNA levels of those transferases involved in the biosynthetic pathways of GlcNAc-branched *N*-glycans showed no significant differences at indicated times in the WT cells. We speculated that diverse environmental cues such as cell adhesion and the cell cycle during the timepoints may influence the glycosylation and secretory pathways of glycoproteins and their expression levels. The underlying molecular mechanism will require further study.

This study also showed that SLC35A3 may not be one of the main UDP-GlcNAc transporters for *N*-glycosylation, since the biosynthesis of bi-antennary *N*-glycans was not significantly blocked in the SLC35A3-KO cells. The recent study by Bożena Szulc et al. also came to a similar conclusion; they also speculated that SLC35A3 is not the main supplier of UDP-GlcNAc for *N*-glycosylation and speculated there is a more efficient multi-protein complex that functions as a single transporter of UDP-GlcNAc for *N*-glycosylation (63). In addition, SLC35A3 has been reported to either directly or indirectly interact with SLC35A2 (58), SLC35A4 (64), GnT-IV (62), and GnT-V (55, 62, 64), and the interactions among glycosyltransferases and nucleotide sugar transporters to form multi-enzyme/multi-transporter complexes in the Golgi membranes may facilitate the efficient synthesis of complex *N*-glycans (64). It is also possible, however, that some Golgi-resident nucleotide sugar transporters may specifically serve corresponding glycosyltransferases. For example, SLC35A2 interacts with B4GalT1, which is widely expressed in all tissues and is considered quite important in the galactosylation of *N*-glycans. Also, a deficiency in either SLC35A2 or B4GalT1 results in a significant lack of galactose moieties on *N*-glycans (65-67).

Emerging data have clearly shown that *O*-GlcNAcylation plays critical roles in the progress of human diseases, particularly diseases such as cancers, diabetes, and Alzheimer's disease (25, 32-34). The regulation of *O*-GlcNAcylation may be directly involved in diabetes. OGT and *O*-GlcNAc-modified protein levels are increased in the pancreatic islets, as well as in the tissues of the sciatic nerve, kidney, and liver in diabetic rats (68). Curiously, a decrease in *O*-GlcNAcylation caused by the overexpression of OGA in the pancreatic β cells of transgenic mice led to a decrease in insulin secretion (69). On the other hand, it is well known that a loss

of GnT-IV inhibits GlcNAc-branching formation on Glut-2, which decreases Glut-2 stability on the cell surface and promotes its endocytosis, which decreases insulin secretion and results in the pathogenesis of type 2 diabetes in mice (12). Based on these observations together with the results of this study, it would be very interesting to investigate the relationship between *O*-GlcNAcylation and Glut-2 expression on the cell surface.

Cell migration is a central process in the development and maintenance of multicellular organisms (70). In the previous study, we found that the suppression of *O*-GlcNAcylation inhibited integrin-mediated cell migration due to an aberrant increase in cell-ECM adhesion via an enhancement of focal-adhesion plaque formation (54). The present study also revealed another potential mechanism whereby *O*-GlcNAcylation could regulate the modification of GlcNAc-branched *N*-glycans on membrane proteins such as integrins in order to govern cell migration. Therefore, it will be very important for glycobiology to examine the effects of both *O*-GlcNAcylation and *N*-glycosylation rather than focusing on one or the other.

5. References

1. Gabius, H. J. (2018) The sugar code: Why glycans are so important. *BioSyst.* **164**, 102-111
2. Reily, C., Stewart, T. J., Renfrow, M. B., and Novak, J. (2019) Glycosylation in health and disease. *Nature reviews. Nephrology* **15**, 346-366
3. Ohtsubo, K., and Marth, J. D. (2006) Glycosylation in cellular mechanisms of health and disease. *Cell* **126**, 855-867
4. Varki, A., Kannagi, R., Toole, B., and Stanley, P. (2015) Glycosylation Changes in Cancer. In *Essentials of Glycobiology* (Varki, A., Cummings, R. D., Esko, J. D., Stanley, P., Hart, G. W., Aebi, M., Darvill, A. G., Kinoshita, T., Packer, N. H., Prestegard, J. H., Schnaar, R. L., and Seeberger, P. H., eds) pp. 597-609, Cold Spring Harbor Laboratory Press Copyright 2015-2017 by The Consortium of Glycobiology Editors, La Jolla, California. All rights reserved., Cold Spring Harbor (NY)
5. Rudman, N., Gornik, O., and Lauc, G. (2019) Altered N-glycosylation profiles as potential biomarkers and drug targets in diabetes. *FEBS letters* **593**, 1598-1615
6. Sun, S., Hu, Y., Ao, M., Shah, P., Chen, J., Yang, W., Jia, X., Tian, Y., Thomas, S., and Zhang, H. (2019) N-GlycositeAtlas: a database resource for mass spectrometry-based human N-linked glycoprotein and glycosylation site mapping. *Clinical proteomics* **16**, 35
7. Zhao, Y. Y., Takahashi, M., Gu, J. G., Miyoshi, E., Matsumoto, A., Kitazume, S., and Taniguchi, N. (2008) Functional roles of N-glycans in cell signaling and cell adhesion in cancer. *Cancer Sci.* **99**, 1304-1310
8. Yoshida, Y., and Tanaka, K. (2018) Cytosolic N-Glycans: Triggers for Ubiquitination Directing Proteasomal and Autophagic Degradation. **40**, 1700215
9. Yoshida, Y., Mizushima, T., and Tanaka, K. (2019) Sugar-Recognizing Ubiquitin Ligases: Action Mechanisms and Physiology. *Frontiers in physiology* **10**, 104
10. Yoshimura, M., Ihara, Y., Matsuzawa, Y., and Taniguchi, N. (1996) Aberrant glycosylation of E-cadherin enhances cell-cell binding to suppress metastasis. *J Biol Chem* **271**, 13811-13815
11. Kitada, T., Miyoshi, E., Noda, K., Higashiyama, S., Ihara, H., Matsuura, N., Hayashi, N., Kawata, S., Matsuzawa, Y., and Taniguchi, N. (2001) The addition of bisecting N-acetylglucosamine residues to E-cadherin down-regulates the tyrosine phosphorylation of beta-catenin. *J Biol Chem* **276**, 475-480
12. Ohtsubo, K., Takamatsu, S., Minowa, M. T., Yoshida, A., Takeuchi, M., and Marth, J. D. (2005) Dietary and genetic control of glucose transporter 2 glycosylation promotes insulin secretion in suppressing diabetes. *Cell* **123**, 1307-1321

13. Ohtsubo, K., Chen, M. Z., Olefsky, J. M., and Marth, J. D. (2011) Pathway to diabetes through attenuation of pancreatic beta cell glycosylation and glucose transport. *Nat. Med.* **17**, 1067-1075
14. Schachter, H. (1986) Biosynthetic controls that determine the branching and microheterogeneity of protein-bound oligosaccharides. *Biochem. Cell Biol.* **64**, 163-181
15. Kizuka, Y., and Taniguchi, N. (2016) Enzymes for N-Glycan Branching and Their Genetic and Nongenetic Regulation in Cancer. *Biomolecules* **6**, 25
16. Niimi, K., Yamamoto, E., Fujiwara, S., Shinjo, K., Kotani, T., Umezu, T., Kajiyama, H., Shibata, K., Ino, K., and Kikkawa, F. (2012) High expression of N-acetylglucosaminyltransferase IVa promotes invasion of choriocarcinoma. *Br. J. Cancer* **107**, 1969-1977
17. Fan, J., Wang, S., Yu, S., He, J., Zheng, W., and Zhang, J. (2012) N-acetylglucosaminyltransferase IVa regulates metastatic potential of mouse hepatocarcinoma cells through glycosylation of CD147. *Glycoconjugate journal* **29**, 323-334
18. Ide, Y., Miyoshi, E., Nakagawa, T., Gu, J., Tanemura, M., Nishida, T., Ito, T., Yamamoto, H., Kozutsumi, Y., and Taniguchi, N. (2006) Aberrant expression of N-acetylglucosaminyltransferase-IVa and IVb (GnT-IVa and b) in pancreatic cancer. *Biochem Biophys Res Commun* **341**, 478-482
19. Wellen, K. E., and Thompson, C. B. (2010) Cellular metabolic stress: considering how cells respond to nutrient excess. *Mol Cell* **40**, 323-332
20. Biwi, J., Biot, C., Guerardel, Y., Vercoutter-Edouart, A.-S., and Lefebvre, T. (2018) The Many Ways by Which O-GlcNAcylation May Orchestrate the Diversity of Complex Glycosylations. *Molecules (Basel, Switzerland)* **23**, 2858
21. Hart, G. W., Housley, M. P., and Slawson, C. (2007) Cycling of O-linked beta-N-acetylglucosamine on nucleocytoplasmic proteins. *Nature* **446**, 1017-1022
22. Bond, M. R., and Hanover, J. A. (2015) A little sugar goes a long way: the cell biology of O-GlcNAc. *J Cell Biol* **208**, 869-880
23. Hart, G. W. (1997) Dynamic O-linked glycosylation of nuclear and cytoskeletal proteins. *Annu Rev Biochem* **66**, 315-335
24. Simanek, E. E., Huang, D.-H., Pasternack, L., Machajewski, T. D., Seitz, O., Millar, D. S., Dyson, H. J., and Wong, C.-H. (1998) Glycosylation of Threonine of the Repeating Unit of RNA Polymerase II with β -Linked N-Acetylglucosamine Leads to a Turnlike Structure. *J. Am. Chem. Soc.* **120**, 11567-11575
25. Hart, G. W., Slawson, C., Ramirez-Correa, G., and Lagerlof, O. (2011) Cross talk between O-GlcNAcylation and phosphorylation: roles in signaling, transcription, and chronic disease. *Annu Rev Biochem* **80**, 825-858

26. Liu, C., Shi, Y., Li, J., Liu, X., Xiahou, Z., Tan, Z., Chen, X., and Li, J. (2020) O-GlcNAcylation of myosin phosphatase targeting subunit 1 (MYPT1) dictates timely disjunction of centrosomes. *J Biol Chem* **295**, 7341-7349
27. Yang, X., Su, K., Roos, M. D., Chang, Q., Paterson, A. J., and Kudlow, J. E. (2001) O-linkage of N-acetylglucosamine to Sp1 activation domain inhibits its transcriptional capability. *Proc Natl Acad Sci U S A* **98**, 6611-6616
28. Yang, X., and Qian, K. (2017) Protein O-GlcNAcylation: emerging mechanisms and functions. *Nat Rev Mol Cell Biol* **18**, 452-465
29. Gewinner, C., Hart, G., Zachara, N., Cole, R., Beisenherz-Huss, C., and Groner, B. (2004) The coactivator of transcription CREB-binding protein interacts preferentially with the glycosylated form of Stat5. *J Biol Chem* **279**, 3563-3572
30. Chu, C. S., Lo, P. W., Yeh, Y. H., Hsu, P. H., Peng, S. H., Teng, Y. C., Kang, M. L., Wong, C. H., and Juan, L. J. (2014) O-GlcNAcylation regulates EZH2 protein stability and function. *Proc Natl Acad Sci U S A* **111**, 1355-1360
31. Yang, W. H., Kim, J. E., Nam, H. W., Ju, J. W., Kim, H. S., Kim, Y. S., and Cho, J. W. (2006) Modification of p53 with O-linked N-acetylglucosamine regulates p53 activity and stability. *Nat Cell Biol* **8**, 1074-1083
32. Copeland, R. J., Han, G., and Hart, G. W. (2013) O-GlcNAcomics--Revealing roles of O-GlcNAcylation in disease mechanisms and development of potential diagnostics. *Proteomics. Clinical applications* **7**, 597-606
33. Kamigaito, T., Okaneya, T., Kawakubo, M., Shimojo, H., Nishizawa, O., and Nakayama, J. (2014) Overexpression of O-GlcNAc by prostate cancer cells is significantly associated with poor prognosis of patients. *Prostate cancer and prostatic diseases* **17**, 18-22
34. Zhao, L., Shah, J. A., Cai, Y., and Jin, J. (2018) 'O-GlcNAc Code' Mediated Biological Functions of Downstream Proteins. *Molecules (Basel, Switzerland)* **23**, 1967
35. Gu, Y., Gao, J., Han, C., Zhang, X., Liu, H., Ma, L., Sun, X., and Yu, W. (2014) O-GlcNAcylation is increased in prostate cancer tissues and enhances malignancy of prostate cancer cells. *Molecular medicine reports* **10**, 897-904
36. Shi, Y., Tomic, J., Wen, F., Shaha, S., Bahlo, A., Harrison, R., Dennis, J. W., Williams, R., Gross, B. J., Walker, S., Zuccolo, J., Deans, J. P., Hart, G. W., and Spaner, D. E. (2010) Aberrant O-GlcNAcylation characterizes chronic lymphocytic leukemia. *Leukemia* **24**, 1588-1598
37. Ferrer, C. M., Lynch, T. P., Sodi, V. L., Falcone, J. N., Schwab, L. P., Peacock, D. L., Vocadlo, D. J., Seagroves, T. N., and Reginato, M. J. (2014) O-GlcNAcylation regulates cancer metabolism and survival stress signaling via regulation of the HIF-1 pathway. *Mol Cell* **54**, 820-831

38. Zhu, Q., Zhou, L., Yang, Z., Lai, M., Xie, H., Wu, L., Xing, C., Zhang, F., and Zheng, S. (2012) O-GlcNAcylation plays a role in tumor recurrence of hepatocellular carcinoma following liver transplantation. *Medical oncology (Northwood, London, England)* **29**, 985-993
39. Ma, Z., Vocadlo, D. J., and Vosseller, K. (2013) Hyper-O-GlcNAcylation is anti-apoptotic and maintains constitutive NF- κ B activity in pancreatic cancer cells. *J Biol Chem* **288**, 15121-15130
40. Xu, D., Wang, W., Bian, T., Yang, W., Shao, M., and Yang, H. (2019) Increased expression of O-GlcNAc transferase (OGT) is a biomarker for poor prognosis and allows tumorigenesis and invasion in colon cancer. *International journal of clinical and experimental pathology* **12**, 1305-1314
41. Gu, Y., Mi, W., Ge, Y., Liu, H., Fan, Q., Han, C., Yang, J., Han, F., Lu, X., and Yu, W. (2010) GlcNAcylation plays an essential role in breast cancer metastasis. *Cancer Res* **70**, 6344-6351
42. Peterson, S. B., and Hart, G. W. (2016) New insights: A role for O-GlcNAcylation in diabetic complications. *Crit. Rev. Biochem. Mol. Biol.* **51**, 150-161
43. Lau, K. S., Partridge, E. A., Grigorian, A., Silvescu, C. I., Reinhold, V. N., Demetriou, M., and Dennis, J. W. (2007) Complex N-glycan number and degree of branching cooperate to regulate cell proliferation and differentiation. *Cell* **129**, 123-134
44. Ghosh, S. K., Bond, M. R., Love, D. C., Ashwell, G. G., Krause, M. W., and Hanover, J. A. (2014) Disruption of O-GlcNAc Cycling in *C. elegans* Perturbs Nucleotide Sugar Pools and Complex Glycans. *Front Endocrinol (Lausanne)* **5**, 197
45. Sato, Y., Isaji, T., Tajiri, M., Yoshida-Yamamoto, S., Yoshinaka, T., Somehara, T., Fukuda, T., Wada, Y., and Gu, J. (2009) An N-glycosylation site on the beta-propeller domain of the integrin α 5 subunit plays key roles in both its function and site-specific modification by beta1,4-N-acetylglucosaminyltransferase III. *J Biol Chem* **284**, 11873-11881
46. Isaji, T., Im, S., Gu, W., Wang, Y., Hang, Q., Lu, J., Fukuda, T., Hashii, N., Takakura, D., Kawasaki, N., Miyoshi, H., and Gu, J. (2014) An oncogenic protein Golgi phosphoprotein 3 up-regulates cell migration via sialylation. *J Biol Chem* **289**, 20694-20705
47. Tanabe, K., and Ikenaka, K. (2006) In-column removal of hydrazine and N-acetylation of oligosaccharides released by hydrazinolysis. *Anal. Biochem.* **348**, 324-326
48. Tomiya, N., Awaya, J., Kurono, M., Endo, S., Arata, Y., and Takahashi, N. (1988) Analyses of N-linked oligosaccharides using a two-dimensional mapping technique. *Anal. Biochem.* **171**, 73-90
49. Tomiya, N., Lee, Y. C., Yoshida, T., Wada, Y., Awaya, J., Kurono, M., and Takahashi, N. (1991) Calculated two-dimensional sugar map of pyridylaminated oligosaccharides:

- elucidation of the jack bean alpha-mannosidase digestion pathway of Man9GlcNAc2. *Anal. Biochem.* **193**, 90-100
50. Kao, S.-H., Wang, W.-L., Chen, C.-Y., Chang, Y.-L., Wu, Y.-Y., Wang, Y.-T., Wang, S.-P., Nesvizhskii, A. I., Chen, Y.-J., Hong, T.-M., and Yang, P.-C. (2015) Analysis of Protein Stability by the Cycloheximide Chase Assay. *Bio-protocol* **5**, e1374
 51. Sanjana, N. E., Shalem, O., and Zhang, F. (2014) Improved vectors and genome-wide libraries for CRISPR screening. *Nat. Methods* **11**, 783-784
 52. Shalem, O., Sanjana, N. E., Hartenian, E., Shi, X., Scott, D. A., Mikkelsen, T., Heckl, D., Ebert, B. L., Root, D. E., Doench, J. G., and Zhang, F. (2014) Genome-scale CRISPR-Cas9 knockout screening in human cells. *Science* **343**, 84-87
 53. Takamatsu, S., Korekane, H., Ohtsubo, K., Oguri, S., Park, J. Y., Matsumoto, A., and Taniguchi, N. (2013) N-Acetylglucosaminyltransferase (GnT) Assays Using Fluorescent Oligosaccharide Acceptor Substrates: GnT-III, IV, V, and IX (GnT-Vb). In *Glycosyltransferases: Methods and Protocols* (Brockhausen, I., ed) pp. 283-298, Humana Press, Totowa, NJ
 54. Xu, Z., Isaji, T., Fukuda, T., Wang, Y., and Gu, J. (2019) O-GlcNAcylation regulates integrin-mediated cell adhesion and migration via formation of focal adhesion complexes. *J Biol Chem* **294**, 3117-3124
 55. Maszczak-Seneczko, D., Sosicka, P., Olczak, T., Jakimowicz, P., Majkowski, M., and Olczak, M. (2013) UDP-N-acetylglucosamine transporter (SLC35A3) regulates biosynthesis of highly branched N-glycans and keratan sulfate. *J Biol Chem* **288**, 21850-21860
 56. Edvardson, S., Ashikov, A., Jalas, C., Sturiale, L., Shaag, A., Fedick, A., Treff, N. R., Garozzo, D., Gerardy-Schahn, R., and Elpeleg, O. (2013) Mutations in SLC35A3 cause autism spectrum disorder, epilepsy and arthrogryposis. *J. Med. Genet.* **50**, 733-739
 57. Toscanini, M. A., Favaro, M. B., Gonzalez Flecha, F. L., Ebert, B., Rautengarten, C., and Bredeston, L. M. (2019) Conserved Glu-47 and Lys-50 residues are critical for UDP-N-acetylglucosamine/UMP antiport activity of the mouse Golgi-associated transporter Slc35a3. *J Biol Chem* **294**, 10042-10054
 58. Maszczak-Seneczko, D., Sosicka, P., Majkowski, M., Olczak, T., and Olczak, M. (2012) UDP-N-acetylglucosamine transporter and UDP-galactose transporter form heterologous complexes in the Golgi membrane. *FEBS letters* **586**, 4082-4087
 59. Oguri, S., Yoshida, A., Minowa, M. T., and Takeuchi, M. (2006) Kinetic properties and substrate specificities of two recombinant human N-acetylglucosaminyltransferase-IV isozymes. *Glycoconjugate journal* **23**, 473-480
 60. Takamatsu, S., Antonopoulos, A., Ohtsubo, K., Ditto, D., Chiba, Y., Le, D. T., Morris, H. R., Haslam, S. M., Dell, A., Marth, J. D., and Taniguchi, N. (2010) Physiological and

- glycomic characterization of N-acetylglucosaminyltransferase-IVa and -IVb double deficient mice. *Glycobiology* **20**, 485-497
61. Lau, K. S., and Dennis, J. W. (2008) N-Glycans in cancer progression. *Glycobiology* **18**, 750-760
62. Maszczak-Seneczko, D., Sosicka, P., Kaczmarek, B., Majkowski, M., Luzarowski, M., Olczak, T., and Olczak, M. (2015) UDP-galactose (SLC35A2) and UDP-N-acetylglucosamine (SLC35A3) Transporters Form Glycosylation-related Complexes with Mannoside Acetylglucosaminyltransferases (Mgats). *J Biol Chem* **290**, 15475-15486
63. Szulc, B., Sosicka, P., Maszczak-Seneczko, D., Skurska, E., Shauchuk, A., Olczak, T., Freeze, H. H., and Olczak, M. (2020) Biosynthesis of GlcNAc-rich N- and O-glycans in the Golgi apparatus does not require the nucleotide sugar transporter SLC35A3. *J. Biol. Chem.* **295**, 16445-16463
64. Khoder-Agha, F., Sosicka, P., Escriva Conde, M., Hassinen, A., Glumoff, T., Olczak, M., and Kellokumpu, S. (2019) N-acetylglucosaminyltransferases and nucleotide sugar transporters form multi-enzyme-multi-transporter assemblies in golgi membranes in vivo. *Cell. Mol. Life Sci.* **76**, 1821-1832
65. Wiertelak, W., Sosicka, P., Olczak, M., and Maszczak-Seneczko, D. (2020) Analysis of homologous and heterologous interactions between UDP-galactose transporter and beta-1,4-galactosyltransferase 1 using NanoBiT. *Anal. Biochem.* **593**, 113599
66. Guo, S., Sato, T., Shirane, K., and Furukawa, K. (2001) Galactosylation of N-linked oligosaccharides by human beta-1,4-galactosyltransferases I, II, III, IV, V, and VI expressed in Sf-9 cells. *Glycobiology* **11**, 813-820
67. Guillard, M., Morava, E., de Ruijter, J., Roscioli, T., Penzien, J., van den Heuvel, L., Willemsen, M. A., de Brouwer, A., Bodamer, O. A., Wevers, R. A., and Lefeber, D. J. (2011) B4GALT1-congenital disorders of glycosylation presents as a non-neurologic glycosylation disorder with hepatointestinal involvement. *The Journal of pediatrics* **159**, 1041-1043.e1042
68. Akimoto, Y., Hart, G. W., Wells, L., Vosseller, K., Yamamoto, K., Munetomo, E., Ohara-Imaizumi, M., Nishiwaki, C., Nagamatsu, S., Hirano, H., and Kawakami, H. (2007) Elevation of the post-translational modification of proteins by O-linked N-acetylglucosamine leads to deterioration of the glucose-stimulated insulin secretion in the pancreas of diabetic Goto-Kakizaki rats. *Glycobiology* **17**, 127-140
69. Soesanto, Y., Luo, B., Parker, G., Jones, D., Cooksey, R. C., and McClain, D. A. (2011) Pleiotropic and age-dependent effects of decreased protein modification by O-linked N-acetylglucosamine on pancreatic β -cell function and vascularization. *J Biol Chem* **286**, 26118-26126

70. Franz, C. M., Jones, G. E., and Ridley, A. J. (2002) Cell migration in development and disease. *Dev Cell* **2**, 153-158

6. Abbreviations

2-AB, 2-aminobenzamide; CRISPR/Cas-9, clustered regularly interspaced short palindromic repeats/caspase-9; DMEM, Dulbecco's modified Eagle's medium; DOX, doxycycline; FBS, fetal bovine serum; GAPDH, glyceraldehyde-3-phosphate dehydrogenase; GnGnbi-PA, pyridylamine-labeled GlcNAc-terminated bi-antennary glycan; GnT-IV, *N*-acetylglucosaminyltransferase IV; GnT-V, *N*-acetylglucosaminyltransferase V; GU, glucose units; HBP, hexosamine biosynthetic pathway; KD, knockdown; KO, knockout; PBS, phosphate buffered saline; shRNA, short hairpin RNA; UDP-GlcNAc, diphosphate β -D-*N*-acetylglucosamine; VSV, vesicular stomatitis virus glycoprotein; WT, wild type.

7. Acknowledgments

First of all, I owe my sincerely gratitude to President Motoaki Takayanagi to provide the opportunity of studying in Tohoku Medical and Pharmaceutical University.

I would like to show my gratitude to my supervisor, Prof. Jianguo Gu. This thesis would not have been possible unless Prof. Gu designed the project, analyzed the data and revised the manuscript.

I would like to thank Dr. Tomoya Isaji for the guidance and design on the experiments. Many thanks for Dr. Tomohiko Fukuda to provide technique helps. Thanks for the helps from Ms. Caixia Liang, Mr. Chengwei Duan, Ms. Jie Yang, Mr. Feng Qi, Mr. Xing Xu, Mr. Jianwei Liu, Ms. Yuhan Sun and Ms. Yan Hao.

Finally, I would like thank my family and all those people who have, directly or indirectly, made efforts and contributions to completion of this dissertation.